Soft Matter

Formation of high aspect ratio wrinkles and ridges on elastic bilayers with small thickness contrast

Journal:	*Soft Matter*
Manuscript ID	SM-ART-07-2018-001345.R1
Article Type:	Paper
Date Submitted by the Author:	13-Sep-2018
Complete List of Authors:	Auguste, Anesia; University of Massachusetts Amherst, Polymer Science and Engineering Yang, Jiawei; Harvard University , School of Engineering and Applied Sciences Jin, Lihua; UCLA Division of Physical Sciences, Mechanical and Aerospace Engineering Chen, Dayong; UCLA Division of Physical Sciences, Mechanical and Aerospace Engineering Suo, Zhigang; Harvard University , Hayward, Ryan; University of Massaschusetts, Polymer Science and Engineering

Formation of high aspect ratio wrinkles and ridges on elastic bilayers with small thickness contrast

Anesia Auguste[1], Jiawei Yang[2], Lihua Jin[2], Dayong Chen[1], Zhigang Suo[2], and Ryan C. Hayward[1]

1 Department of Polymer Science & Engineering, University of Massachusetts, Amherst, MA, 01003, USA. *E-mail: hayward@umass.edu

2 School of Engineering and Applied Sciences, Kavli Institute for Nanobio Science and Technology, Harvard University, Cambridge, MA, 02138, USA. *E-mail: suo@seas.harvard.edu

Abstract

An elastic bilayer composed of a stiff film bonded to a soft substrate forms wrinkles under compression. While these uniform and periodic wrinkles initially grow in amplitude with applied strain, the onset of secondary bifurcations such as period doubling typically limit the aspect ratio (i.e., amplitude divided by wavelength) of wrinkles that can be achieved. Here, we present a simple strategy that employs a supported bilayer with comparable thicknesses of the film and substrate to achieve wrinkles with higher aspect ratio. We use both experiments and finite element simulations to reveal that at small thickness contrast, period doubling can be delayed, allowing the wrinkles to grow uniformly to high aspect ratio. In addition, we show that the periodic wrinkles can evolve through a symmetry breaking and transition to a periodic pattern of ridges with even higher aspect ratio.

Introduction

Wrinkles form when an elastic bilayer composed of a stiff film bonded to a soft substrate is compressed to beyond a critical strain. The balance between the bending energy of the film and the stretching energy of the substrate selects the well-defined initial wavelength for wrinkles. To date, studies on the formation and evolution of wrinkles have focused largely on scenarios where the substrate is much thicker than the film, usually by at least an order of magnitude (*1*–*5*).

In these scenarios, the wrinkle wavelength and amplitude both scale linearly with the film thickness, but are independent of the substrate thickness (*6*, *7*). As the compressive strain increases, the wrinkle amplitude increases while the wavelength decreases, and therefore the aspect ratio (defined as the ratio of amplitude to wavelength) of the wrinkles rises.

The ability to form wrinkles with high aspect ratios is of growing research interest (*8–12*). For example, high aspect ratio wrinkles are used to build dynamically tunable surfaces with useful optical and wetting characteristics (*13–16*), as well as to improve the stretchability of flexible electronics (*17–19*). Previous work has focused on achieving high aspect ratio wrinkles largely by using a highly pre-stretched substrate, allowing a large amount of compression to be applied to the bilayer. However, such bilayer system tends to undergo secondary elastic bifurcations such as period doubling and creasing (*3*, *20*, *21*), or failure modes such as cracking and delamination (*22*, *23*), setting an upper limit to the aspect ratio which can be achieved while maintaining regularity of the amplitudes for each surface feature, an important requirement for many applications. While these processes typically limit the achievable aspect ratio to ~ 0.35, careful tuning of the substrate pre-stretch and modulus has been shown to delay secondary bifurcations, yielding wrinkles with an aspect ratio as high as 0.65 (*10*).

A less studied scenario is when the substrate thickness, H_s, approaches the thickness of the film, $H_{f,}$, which holds relevance for flexible electronic devices (*17–19*) and many biological tissues (*24*, *25*). As the substrate thickness becomes comparable to the film thickness, bending of the film is increasingly constrained, thereby delaying wrinkle formation to larger strains, and reducing the initial wrinkle wavelength and amplitude (*26*, *27*). However, little research has been devoted to understanding the effects of the thickness contrast (H_s/H_f) on the aspect ratio of wrinkles. In this paper, we exploit the constraining effect of a thin substrate to delay secondary

bifurcations and show that a substrate thickness of only several times the film thickness allows for aspect ratios up to 0.67 to be achieved. Furthermore, by harnessing the transition of wrinkles to periodic ridges through a symmetry-breaking process, an even higher aspect ratio of 1.13 can be achieved.

Methods

Experimental

Uniform uniaxial compression is applied to elastic bilayers by bonding to an underlying pre-stretched mounting layer. In detail, a 1-mm-thick silica-reinforced vinyl-terminated polydimethylsiloxane (PDMS) mounting layer (Elastosil M4600, Wacker Chemical Company, shear modulus of 232 ± 10 kPa) is uniaxially pre-stretched on a stretcher. The film is prepared by spin coating uncured PDMS (Sylgard 184, Dow Corning) comprising 5:1 by weight of base to crosslinker (yielding a shear modulus G_f = 0.87 ± 0.27 MPa) (*28*) and 4.5 μg of fluorescein-o-acrylate in 1,4-dioxane onto a trimethylchlorosiloxane treated glass slide and then placed in the oven at 120 ºC for 2 h to cure. To form the substrate, uncured PDMS with a 40:1 base to crosslinker ratio (yielding a shear modulus G_s = 16 kPa) (*29*) is spin-coated on top of the 5:1 PDMS coated glass slide, and placed in an oven at 120 ºC for 10 min to partially cure. This bilayer is then attached to the mounting layer and placed in an oven at 40 ºC for 16 h to bond and fully cure the PDMS substrate layer. The resulting bilayer has a modulus contrast (G_f/G_s) of ~50. A range of thicknesses for both the substrate (30 - 90 μm) and film (10 - 35 μm) are achieved by changing the spin-coating speeds. Cross-sectional images are taken by laser scanning confocal fluorescence microscopy (Zeiss LSM 510 Meta) using a 25x variable immersion lens with an index matching fluid consisting of 72% glycerol and 28% water by weight. Optical microscopy

with 5x and 10x objective lenses is used to characterize the shape and dynamics of the wrinkles. In addition, optical profilometry (Zygo NewView 7300) is used to measure the wrinkle amplitude A and wavelength λ. The amplitude is calculated as the distance from the wrinkle peak to the trough divided by two. The aspect ratio is defined as the wrinkle amplitude divided by the wavelength (A/λ).

FEM Simulations

To gain insight into how the contrasts in bilayer thickness and modulus influence the achievable aspect ratios of wrinkles, we use Abaqus 6.12/standard software to conduct finite element simulations. Uniaxial compression is realized by constructing a thin-wall cylinder with inner radius 25 times larger than the bilayer thickness, and the compression is applied at the two ends of the cylinder along the axial direction. The wrinkle pattern forms on the outer surface of the cylinder. A schematic illustration is shown in Figure S1. Since the mounting layer does not deform appreciably during compression in the experiments, we only model the film and substrate bilayer, and represent the mounting layer by imposing boundary conditions to the substrate. Linear perturbation analysis is first performed to determine the wavelength of wrinkles (*30*). For simplicity, we choose the computational cell (unit cell) to be the bilayer system with one wavelength λ. In the simulations, we take both the film and the substrate to be incompressible neo-Hookean materials with shear moduli G_f and G_s, and model them with element type CAX4RH. The bottom boundary of the unit cell is subject to an applied displacement u_o ($o < u_o < \lambda$), so that the applied strain is u_o/λ; the top boundary of the unit cell corresponds to the line of symmetry; on the left boundary of the unit cell, the horizontal displacement is enforced to

be uniform, and the vertical displacement is linearly distributed $u_o x/\lambda$. Here x is the vertical coordinate along the left boundary with the origin at the line of symmetry (Figure S1). We perturb the right surface of the unit cell into a sinusoidal shape, with wavelength λ and very small amplitude 0.001 H_s (*31*, *32*). To trigger period doubling, a linear displacement in the range $0 < x < \lambda/10$ is superimposed onto the sinusoidal shape with amplitude 0.0001 H_s at the left boundary of the free surface and amplitude 0 at $x = \lambda/10$.

The simulation method for ridges is similar to wrinkles. The computational cell is at least 5 wavelengths. Since the ridge mode is localized, we prescribe an initial deformation mode of ridge shape. The choice of such deformation mode is not unique, but here we choose an exponential form (*31*, *32*). The initial perturbation is a linear combination of a sinusoidal mode with periodicity matching the wrinkle wavelength with amplitude of 0.001 H_s, and an exponential mode of profile exp(x-λ) that decays from an amplitude of 0.0005 H_s at the top boundary ($x = \lambda$) to zero at the bottom boundary ($x = 0$). A ridge is expected to form in the center of the computational cell. To allow the calculation to continue past the transition to the ridge state, artificial damping is employed in the simulation. The specific damping factor is set to 0.0002. The detailed simulation method and discussion of formation of ridges in elastic bilayers can be found in Ref (*32*).

Results and discussion

To understand the influence of thickness contrast between the substrate and film on post-wrinkling bifurcations of compressed bilayers, we first characterize the cross-sectional profile of experimental samples with a thickness contrast ranging from 2 – 10 and a modulus contrast fixed at 50 using confocal and optical microscopy. We restrict our study to a thickness contrast above 2, since smaller values are found to yield deformation of the mounting layer/substrate interface

(meaning that the sample acts as a trilayer instead of a bilayer and thus its behavior becomes more complex). We track the morphology evolution by characterizing the cross-sectional profile with *in situ* confocal and optical microscopy as we apply small step-wise increments of compressive strain.

For a bilayer with large thickness and modulus contrast, wrinkles form at small strains (typically several percent or less), but transition to a period doubled state at a strain of ~ 0.2 (*30*, *31*, *33*). Period doubling involves the formation of a regular pattern where every other wrinkle trough increases in amplitude due to non-linearity of the substrate elasticity which favors inward relative to outward deflections. Due to the onset of the period doubled state, the aspect ratios achieved for wrinkles is generally limited to 0.1 - 0.2 (*10*). In contrast, Figure 1(a) shows that a small thickness contrast ($H_s/H_f = 3$) substantially delays the onset of period doubling. The bilayer forms wrinkles, which grow in amplitude and decrease in wavelength with compression, eventually yielding uniform and large amplitude wrinkles with an aspect ratio of 0.62 ± 0.03, at a strain of 0.44. Afterwards, the wrinkles transition to the period doubled state at a strain of 0.50 ± 0.02. Increasing the thickness contrast dramatically reduces the achievable aspect ratio. For example, when the thickness contrast is 9 (Figure 1b), wrinkles form at a smaller strain and then evolve to the period doubled state at an earlier strain (0.37 ± 0.01), thus limiting the aspect ratio to 0.40 ± 0.02. Finite element simulations agree closely with experiments, as shown in Figure 1 (c - d). For bilayers with thickness contrasts of 3 and 9, respectively, wrinkles form at strains of 0.06 and 0.05 with maximum aspect ratios of 0.62 and 0.44, prior to transitioning to the period doubled state at strains of 0.44 and 0.33.

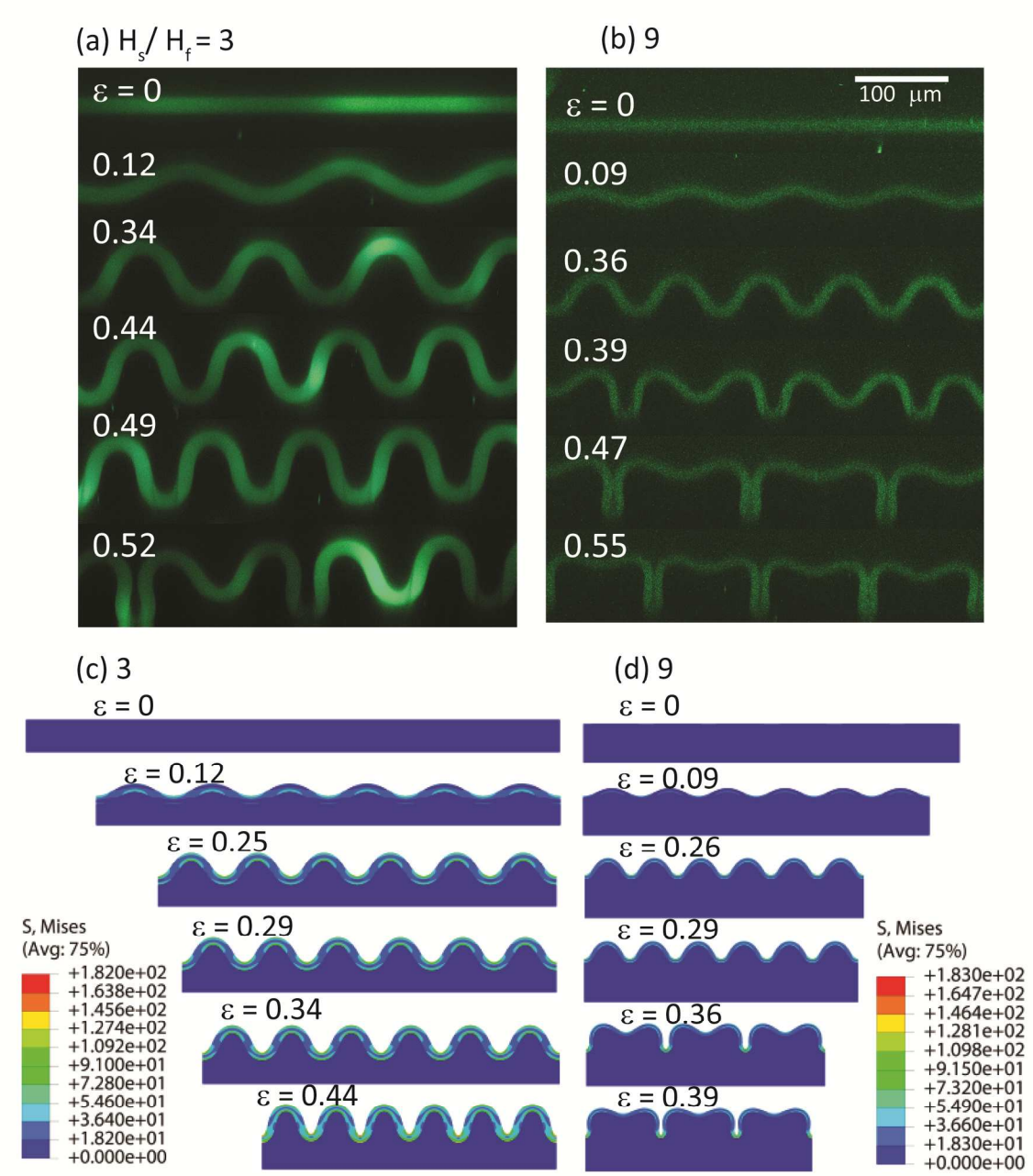

Figure 1. Confocal (a and b) and computational (c and d) cross-sectional views of the evolution of wrinkles to period doubling with thickness contrast of 3 (a and c) and 9 (b and d). The modulus contrast is fixed at 50. The film is fluorescently marked in the confocal cross-sectional views while the substrate is not.

To systematically study how thickness contrast affects the critical strains for wrinkling and period doubling, we conduct experiments and simulations over a range of $2 \leq H_s/H_f \leq 10$ (Figure 2). Experimentally, the critical strain for wrinkling is determined by taking the average

between the strain at which the flat surface is last observed and that at which the wrinkled surface is first detected. These strains also represent the lower and upper bounds of the error bars. The critical strain for period doubling is determined from a plot of the standard deviation of the wrinkle amplitudes versus strain. The point at which the standard deviation begins to increase with a larger slope is taken as the onset of period doubling, as described previously for experiments (*34*) and shown for simulations via the example in Figure S2.

Figure 2(a) shows that the critical strain for wrinkling increases with decreased H_s/H_f. Simulations indicate a value of $\varepsilon_c = 0.09$ at $H_s/H_f = 2$, which decreases to $\varepsilon_c = 0.05$ at $H_s/H_f = 10$, which approaches the value of $\varepsilon_c = 0.25(3E_s/E_f)^{2/3} = 0.038$ in the thick substrate limit. Similar results for the onset of wrinkles at finite thickness contrast have been reported previously (*26*, *27*). Although there is considerable scatter in the experimentally measured values, the data do suggest an increase in critical strain as H_s/H_f is reduced to a value of 2. Further decreases in H_s/H_f provide a very strong constraint from substrate thickness and lead to substantial deformation of the substrate/mounting layer interface, and thus we do not consider this case here.

Figure 2(b) shows that a reduction in H_s/H_f has a more pronounced effect on the critical strain for the secondary bifurcation. In both simulations and experiments, a maximum in the critical strain occurs at $H_s/H_f = 3$ with respective critical strains of 0.44 and 0.50 ± 0.02. Above $H_s/H_f = 3$, the critical strain decreases with increasing H_s/H_f due to a lessening of the constraint

provided by the finite thickness substrate; we expect that this value should eventually asymptote

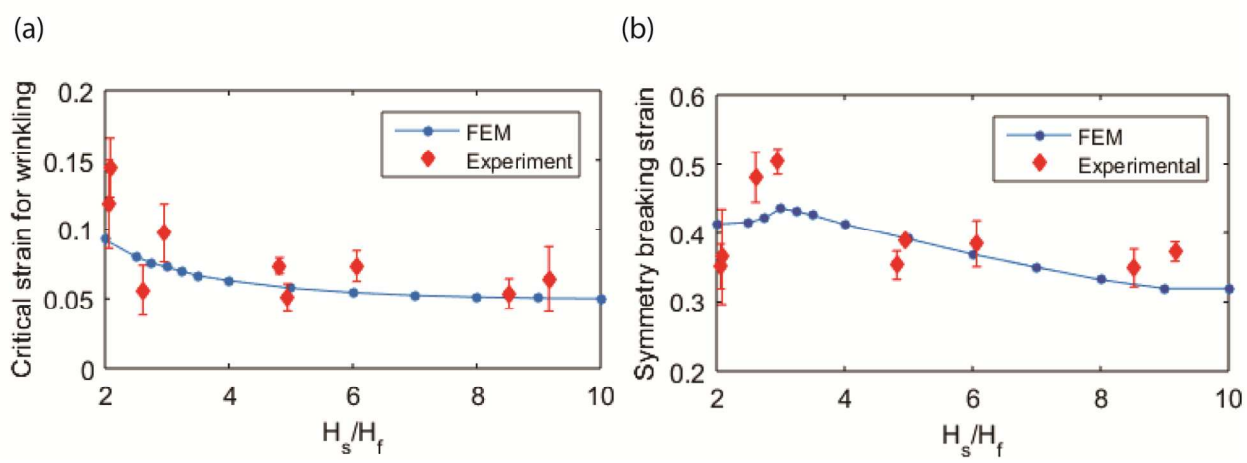

Figure 2. Effect of thickness contrast on critical strain (a) for the onset of wrinkles and (b) for the secondary bifurcations, i.e., period doubling or creasing. The modulus contrast is fixed at 50 for (a) and (b).

to 0.18-0.20 at large H_s/H_f based on previous studies (*21*, *33*, *35*). The increase in critical strain for period doubling at modest H_s/H_f originates from the strong constraint provided by the rigid mounting layer, which increases the energy for 'inward' (towards the substrate), compared to 'outward', deflection of the film. Since period doubling occurs with every second wrinkle trough deepening at the expense of its neighbors, this mode is even more energetically penalized by a thin substrate than is wrinkling. Therefore, period doubling can be substantially delayed. This mechanism is analogous to the effect of substrate pre-stretch on period doubling, where pre-tension is known to soften outward deflection compared to inward deflection and thereby delay period doubling (*31*, *34*), while pre-compression has the opposite effect. Below H_s/H_f =3, however, the critical strain decreases with smaller H_s/H_f. We observe in both experiments and simulations that in this case, the mode of symmetry breaking changes to the uniform formation of creases in every wrinkle trough.

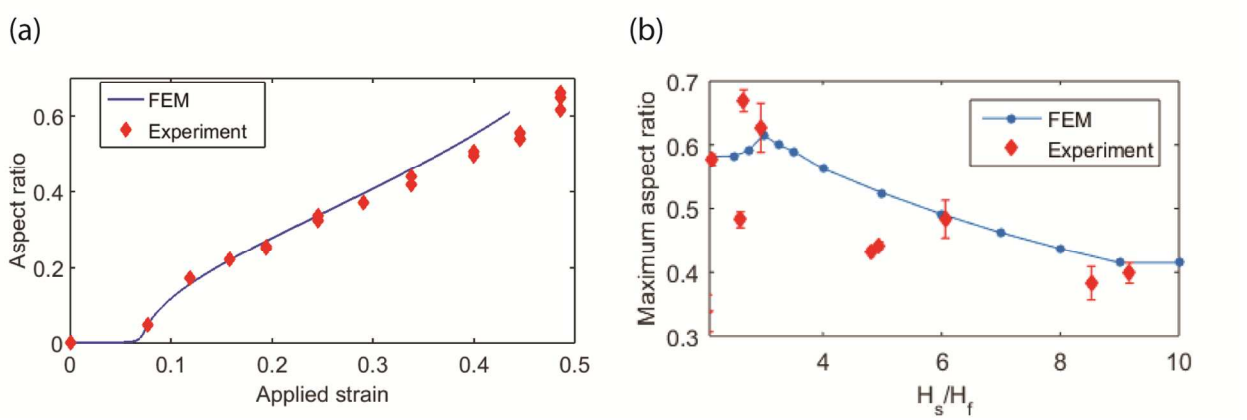

Figure 3. (a) Wrinkle aspect ratio increases with applied strain, as shown here for a thickness contrast of 3 . (b) The maximum aspect ratio attained as function of thickness contrast. The error bars in the y-direction represents the standard deviation of the aspect ratio for at least 4 periods.

We next consider the wrinkle aspect ratio that can be achieved prior to secondary bifurcations. Figure 3(a) shows an example of how aspect ratio evolves with strain for H_s/H_f = 3. For both experiments and simulations, the aspect ratio grows smoothly as the strain increases beyond the critical value of 0.06 for wrinkling, and continues to increase until period doubling sets in. In this case, both experiments and simulations reveal a maximum aspect ratio A_{max} of close to 0.6. The value of A_{max} is plotted vs. thickness contrast in Figure 3(b) for both experiments and simulations. We note that the reported value of A_{max} from experiments is taken at the last strain where the pattern remained regular; since the increment in strain between measurements is as large as 0.05 – 0.07, this may cause the experimental data to systematically underestimate the true value of A_{max}, consistent with the fact that they generally fall below the values predicted by FEM. In both cases, however, the largest value of A_{max} occurs near H_s/H_f = 3. FEM simulations predict that the A_{max} = 0.62, while the highest value observed in experiments is 0.67 ± 0.02. As the thickness contrast increases from 3 to 9, both simulations and experiments show decreases in aspect ratio.

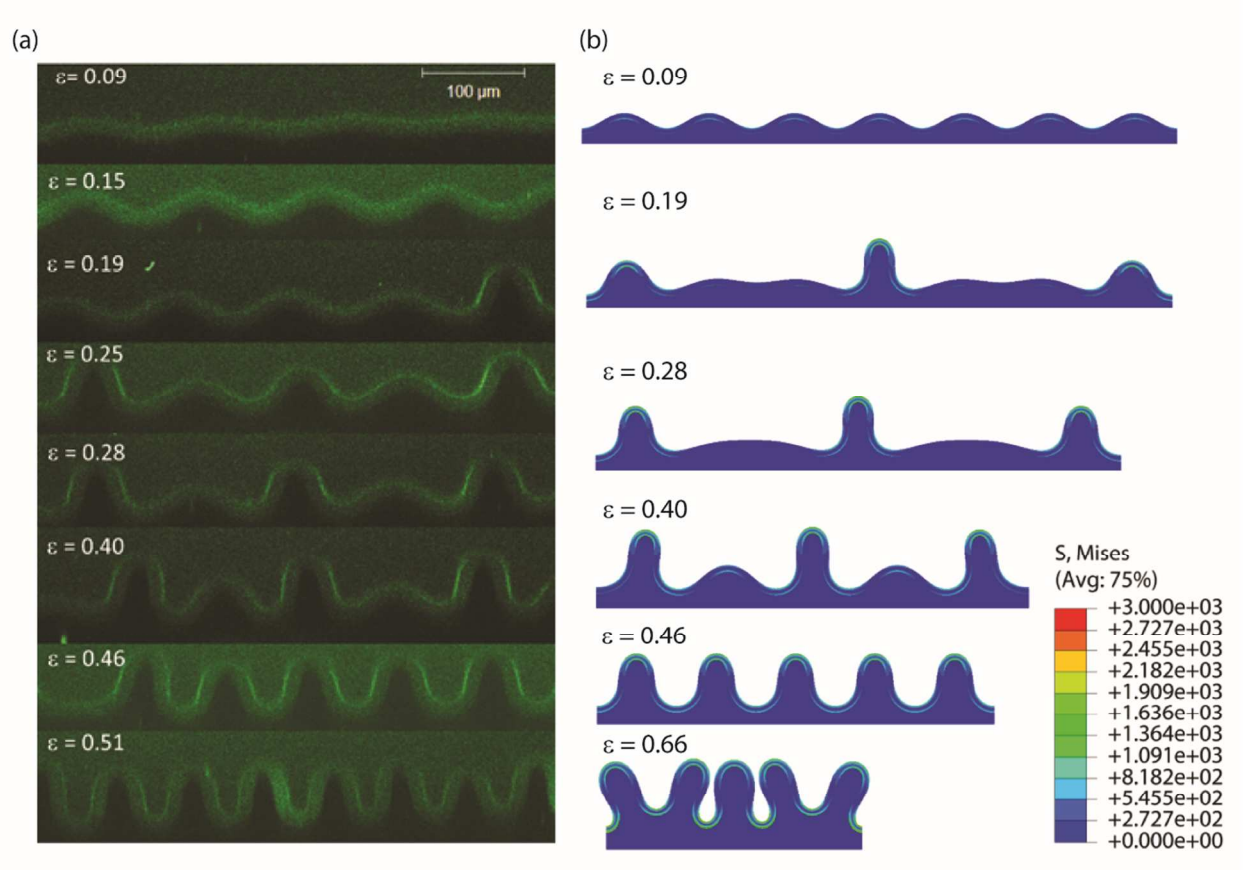

Figure 4. (a) Confocal cross-sectional view and (b) simulation snapshots of the wrinkle to ridge transition for a sample with high modulus contrast (G_f/G_s = 870) and a small thickness contrast (H_s/H_f = 2.5).

The strong confinement effect provided by a thin substrate provides an opportunity to reach even higher aspect ratio surface features through the formation of ridges (*31*). A ridge is another type of secondary bifurcation evolved from wrinkles, corresponding to a localized morphology in which one out of every several wrinkle crests grows outward to very large amplitude compared to the surrounding wrinkles. We achieve formation of ridges by using large modulus contrast but small thickness contrast. As shown in Figure 4, for a sample with a modulus contrast of 870 and a thickness contrast of 2.5, wrinkles undergo several transitions. First, the wrinkles grow in amplitude until a single localized ridge is formed at a strain of 0.19, as the amplitudes of nearby wrinkles decrease. At a strain of 0.25, more wrinkles transform into ridges until all of the ridges evolve into a periodic and uniform pattern at a strain of 0.46. The ridges continue to grow to an aspect ratio of 0.81 ± 0.05 at a strain of 0.51. We note that this is not the maximum achievable aspect ratio, but simply that our current stretching device does not allow for the characterization of samples compressed to greater extents. Once again, this behavior is similar to that reported previously for bilayers with highly pre-stretched substrates (*9*, *36*). Cao and co-workers (*9*) performed finite-element analysis on a bilayer with $G_f/G_s = 1000$ and substrate pre-stretch of $\lambda = 2.0$. They predicted the formation of ridges at a strain of 0.166, followed by an increase in the number of ridges, ultimately leading to uniform structures with aspect ratios of 0.7.

Finite element simulations (Fig. 4b) show similar results, with wrinkles growing uniformly in amplitude until $\varepsilon = 0.12$, after which the center wrinkle increases in amplitude to form a ridge, while the other wrinkles diminish in amplitude. Further compression causes other ridges to form at both ends of the simulation cell. Interestingly, two wrinkles between each ridge coalesce into one wrinkle by $\varepsilon = 0.28$ and then grow into a single ridge, leading to a regular array

of periodic ridges at ε = 0.46. The uniform ridges undergo another bifurcation at a strain of about 0.66 and

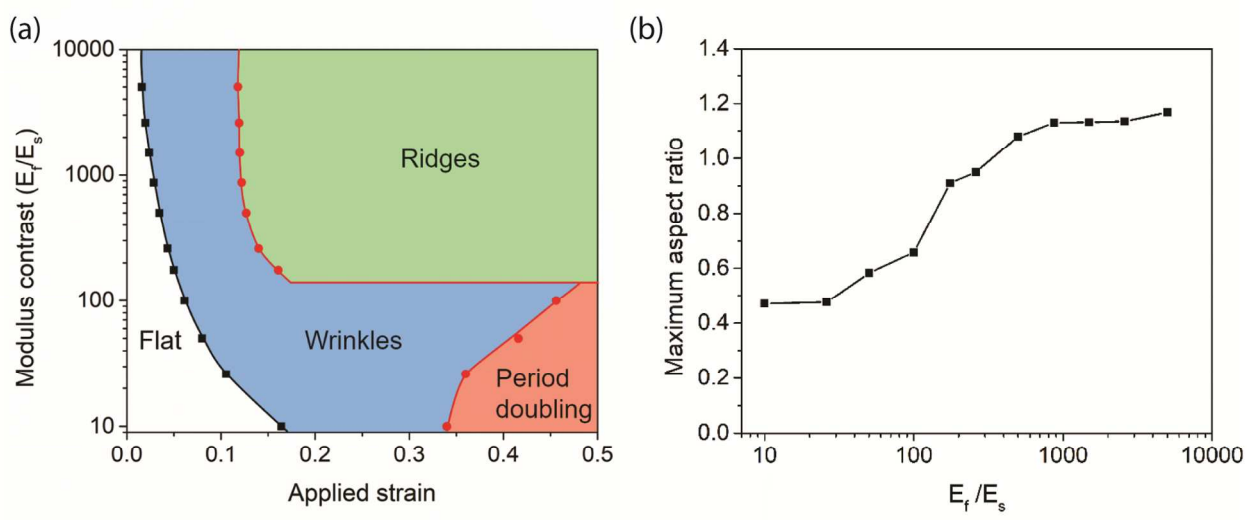

Figure 5. The effect of modulus contrast for a fixed thickness contrast of 2.5. (a) A "phase" diagram from numerical simulations showing the different instability modes with respect to the applied strain and modulus contrast, as well as (b) the maximum aspect ratio of regular features (wrinkles or ridges) achieved in simulations at each value of modulus contrast.

break symmetry again. The maximum achievable aspect ratio for the periodic ridges prior to symmetry breaking is 1.13. However, this transition depends on modulus contrast as shown in Figure 5. As the modulus contrast increase, the wrinkle transitions to ridges instead of the period doubled state (Figure 5a). With that transition to ridges comes a sharp increase in the maximum aspect ratio achieved (Figure 5b), thanks to the tendency of ridges to regain a regular structure at high applied strain (Figure 4). For the highest value studied, $G_f/G_s = 5000$, the highest achievable aspect ratio reaches 1.17 . Such a high aspect ratio has been obtained previously with ridges, but only with very large pre-stretch (9), which may cause failure and thus limit the choice of substrate materials. In this regard, harnessing the wrinkle-to-ridge transition of supported bilayers with modest thickness contrast, but without pre-stretch, may provide a more general route to pattern surfaces with high-aspect-ratio features.

Conclusion

When an elastic bilayer is subjected to compressive strain, the contrast in thickness and modulus between the film and the substrate affect the formation and evolution of surface wrinkles. We show that when the thickness contrast is small (≈ 3), period doubling is delayed due to the strong substrate confinement, leading to high aspect ratio wrinkles. As the thickness contrast becomes larger (> 3), the maximum aspect ratio is reduced. For a modulus contrast of 50, aspect ratios of about 0.65 are found from both experiments and simulations. Furthermore, larger modulus contrasts allow for the formation of uniform ridges with aspect ratios of at least 0.8 achieved in experiments, and 1.17 predicted in simulations. Our strategy provides a simple and robust method to achieve uniform surface patterns with high aspect ratios.

References

1. A. Schweikart, A. Horn, A. Böker, A. Fery, Controlled Wrinkling as a Novel Method for the Fabrication of Patterned Surfaces, 75–99 (2010).
2. C.-C. Lin, F. Yang, S. Lee, Surface wrinkling of an elastic film: effect of residual surface stress. *Langmuir*. **24**, 13627–31 (2008).
3. R. Zhao, T. Zhang, M. Diab, H. Gao, K.-S. Kim, The primary bilayer ruga-phase diagram I: Localizations in ruga evolution. *Extrem. Mech. Lett.* **4**, 76–82 (2015).
4. D. Chen, J. Yoon, D. Chandra, A. J. Crosby, R. C. Hayward, Stimuli-responsive buckling mechanics of polymer films. *J. Polym. Sci. Part B Polym. Phys.* **52**, 1441–1461 (2014).
5. N. Bowden, W. T. S. Huck, K. E. Paul, G. M. Whitesides, The controlled formation of ordered, sinusoidal structures by plasma oxidation of an elastomeric polymer. *Appl. Phys. Lett.* **75**, 2557 (1999).
6. C. M. Stafford *et al.*, A buckling-based metrology for measuring the elastic moduli of polymeric thin films. *Nat. Mater.* **3**, 545–50 (2004).
7. J. Genzer, J. Groenewold, Soft matter with hard skin: From skin wrinkles to templating and material characterization. *Soft Matter*. **2**, 310 (2006).
8. S. F. Ahmed, G.-H. Rho, K.-R. Lee, A. Vaziri, M.-W. Moon, High aspect ratio wrinkles on a soft polymer. *Soft Matter*. **6**, 5709 (2010).
9. C. Cao, H. F. Chan, J. Zang, K. W. Leong, X. Zhao, Harnessing Localized Ridges for High-Aspect-Ratio Hierarchical Patterns with Dynamic Tunability and Multifunctionality. *Adv. Mater.* (2013), doi:10.1002/adma.201304589.
10. Y.-C. Chen, A. J. Crosby, High Aspect Ratio Wrinkles via Substrate Prestretch. *Adv. Mater.* **26**, 5626–5631 (2014).
11. J. G. Gaillard, C. Hendrus, B. D. Vogt, Tunable wrinkle and crease surface morphologies from photoinitiated polymerization of furfuryl alcohol. *Langmuir*. **29**, 15083–9 (2013).
12. Y. Chen, Y. Wang, T. J. Mccarthy, A. J. Crosby, Achieving high aspect ratio wrinkles by modifying material network stress. *Soft Matter*. **13**, 4142–4147 (2017).
13. P.-C. Lin, S. Yang, Mechanically switchable wetting on wrinkled elastomers with dual-scale roughness. *Soft Matter*. **5**, 1011 (2009).
14. S. G. Lee *et al.*, Switchable transparency and wetting of elastomeric smart windows. *Adv. Mater.* **22**, 5013–7 (2010).
15. J. Y. Chung, J. P. Youngblood, C. M. Stafford, Anisotropic wetting on tunable micro-wrinkled surfaces. *Soft Matter*. **3**, 1163 (2007).
16. E. Lee *et al.*, Tilted Pillars on Wrinkled Elastomers as a Reversibly Tunable Optical Window. *Adv. Mater.*, 1–7 (2014).
17. M. S. White *et al.*, Ultrathin, highly flexible and stretchable PLEDs. *Nat. Photonics*. **7**, 811–816 (2013).

18. D.-Y. Khang, H. Jiang, Y. Huang, J. A. Rogers, A stretchable form of single-crystal silicon for high-performance electronics on rubber substrates. *Science*. **311**, 208–12 (2006).

19. J. A. Rogers, T. Someya, Y. Huang, Materials and mechanics for stretchable electronics. *Science*. **327**, 1603–7 (2010).

20. F. Brau, P. Damman, H. Diamant, T. A. Witten, Wrinkle to fold transition: influence of the substrate response. *Soft Matter*. **9**, 8177 (2013).

21. F. Brau *et al.*, Multiple-length-scale elastic instability mimics parametric resonance of nonlinear oscillators. *Nat. Phys.* **7**, 56–60 (2010).

22. Y. Ebata, A. B. Croll, A. J. Crosby, Wrinkling and strain localizations in polymer thin films. *Soft Matter*. **8**, 9086 (2012).

23. Q. Wang, X. Zhao, A three-dimensional phase diagram of growth-induced surface instabilities. *Sci. Rep.* **5**, 8887 (2015).

24. T. Tallinen, J. Y. Chung, J. S. Biggins, L. Mahadevan, Gyrification from constrained cortical expansion. *Proc. Natl. Acad. Sci. U. S. A.* **111**, 12667–72 (2014).

25. B. R. Wiggs, C. A. Hrousis, J. M. Drazen, R. D. Kamm, On the mechanism of mucosal folding in normal and asthmatic airways. *J. Appl. Physiol.* **83**, 1814–1821 (1997).

26. Z. Y. Huang, W. Hong, Z. Suo, Nonlinear analyses of wrinkles in a film bonded to a compliant substrate. *J. Mech. Phys. Solids*. **53**, 2101–2118 (2005).

27. E. Cerda, L. Mahadevan, Geometry and Physics of Wrinkling. *Phys. Rev. Lett.* **90**, 074302 (2003).

28. S. Park, Y. S. Huh, H. G. Craighead, D. Erickson, A method for nanofluidic device prototyping using elastomeric collapse. *Proc. Natl. Acad. Sci. U. S. A.* **106**, 15549–15554 (2009).

29. D. Chen, L. Jin, Z. Suo, R. C. Hayward, Controlled formation and disappearance of creases. *Mater. Horizons*. **1**, 207 (2014).

30. L. Jin, A. Auguste, R. C. Hayward, Z. Suo, Bifurcation diagrams for the formation of wrinkles or creases in soft bilayers. *J. Appl. Mech.* **82**, 1–11 (2015).

31. J. Zang, X. Zhao, Y. Cao, J. W. Hutchinson, Localized ridge wrinkling of stiff films on compliant substrates. *J. Mech. Phys. Solids*. **60**, 1265–1279 (2012).

32. L. Jin, A. Takei, J. W. Hutchinson, Mechanics of wrinkle / ridge transitions in thin film / substrate systems. *J. Mech. Phys. Solids*. **81**, 22–40 (2015).

33. Y. Cao, J. W. Hutchinson, Wrinkling Phenomena in Neo-Hookean Film/Substrate Bilayers. *J. Appl. Mech.* **79**, 031019 (2012).

34. A. Auguste, L. Jin, Z. Suo, R. C. Hayward, The role of substrate pre-stretch in post-wrinkling bifurcations. *Soft Matter*. **10**, 6520–6529 (2014).

35. A. Auguste, L. Jin, Z. Suo, R. C. Hayward, The role of substrate pre-stretch in post-wrinkling bifurcations. *Soft Matter*. **10**, 6520–9 (2014).

36. A. Takei, L. Jin, J. W. Hutchinson, H. Fujita, Ridge Localizations and Networks in Thin Films Compressed by the Incremental Release of a Large Equi-biaxial Pre-stretch in the Substrate. *Adv.*

Mater., 1–7 (2014).